

Optical Detection of Brain Cell Activity Using Plasmonic Gold Nanoparticles

Jiayi Zhang, Tolga Atay, and Arto V. Nurmikko*

Division of Engineering and Department of Physics, Brown University, Providence, Rhode Island 02912

Received June 30, 2008; Revised Manuscript Received November 7, 2008

ABSTRACT

Metal nanoparticles are being actively explored for applications that use localized surface plasmon (LSP) resonance for optical sensing. Here we report an electrostatic field sensing technique which has been applied to detection of mammalian brain cell activity, by optically measuring the cellular potential induced shift in the SP resonance mode of an adjacent planar gold nanoparticle array. An experimental scheme was first devised which enables a quantitative calibration of the field-induced plasmon resonance modulation in air. Hippocampal (brain) neural cells were then grown onto the nanoparticle template and cellular level individual transient signals were detected optically when the chemically triggered neurons switched their potential. Experimental data are compared with calculations using the Drude model for the dielectric response of gold and the Stern model for the metal–electrolyte junction, with good agreement.

Localized surface plasmons (LSP) confined to subwavelength size noble metal nanoparticles possess large optical cross sections which have been thoroughly studied.^{1–3} These excitations are being explored for a wide range of optical sensing applications on the micro- and nanoscale. In this work, we use LSP resonances to demonstrate the detection of cellular activity from specific brain cells during their characteristic electrochemical “switching” (signaling by action potentials)—at a single neuron level of spatial resolution. Traditional neuroscience methodology in recording such activity is by electrical techniques, ranging from thin metal wires to microelectrode arrays,^{4–7} where sensor electrodes are inserted into the cellular medium/tissue. These techniques are widely used in both in vitro and in vivo systems, yet they are invasive to the neural tissue and often electronically noisy. Noninvasive all-optical methods have also been developed, but these mainly use fluorescent tags in the form of membrane potential sensitive dyes.^{8–10} While enabling the detection of single neuron electrical activity, these “staining” techniques have fundamental drawbacks such as induced cell toxicity and the photobleaching of the fluorescent dyes.

In the following, we show how the sensitivity of LSP resonances of metallic nanoparticles to their dielectric constants and the surrounding medium makes it possible to intrinsically record neural cell activity at a single neuron level by optical means. (New methods are important in advancing the understanding of the functional principles of neural microcircuits which underlie the brain’s operations). A most

common type bio/chemical LSP sensor relies on the changes in the local index of refraction, upon the adsorption/absorption of target molecules to the metal surface.¹¹ Recently, it has been demonstrated that propagating surface plasmon resonances in gold thin films can be used to detect the ambient refractive index change when the large sciatic nerve bundle (in a rat’s leg) is electrically stimulated and fires compound action potentials.¹² While such an experiment in the peripheral nervous system is necessary for proof-of-concept,¹³ a localized recording on a single brain neural cell would open the possibility of application in monitoring brain neural activity. By contrast to these techniques, we measure directly the change in a metal nanoparticle’s surface electron density that is induced by the local neural cell’s electric field. The associated change in the dielectric constant can then be observed as a shift in the SP resonance wavelength, an effect demonstrated earlier in a different context and configuration for a gold film/electrolyte interface.¹⁴ Physically, the one requirement in our experimental design is to place a plasmonic sensor “template” in the immediate vicinity of a neural cell membrane, for monitoring neural activity via the resonance change in the transmitted or scattered light with adequate signal–noise ratio in a real time experiment with millisecond temporal precision.

Gold nanoparticles are biologically compatible and can be synthesized either via chemical reactions¹ or by electron-beam lithography (EBL). Lithographic approaches enable fabrication of spatially controlled nanoparticle arrays with flexibility in controlling the optical spectrum of their LSPs.^{2,3} For this reason, we chose to create planar “plasmonic templates”, fabricated on indium tin oxide (ITO)-coated glass

* Corresponding author, Arto_Nurmikko@brown.edu.

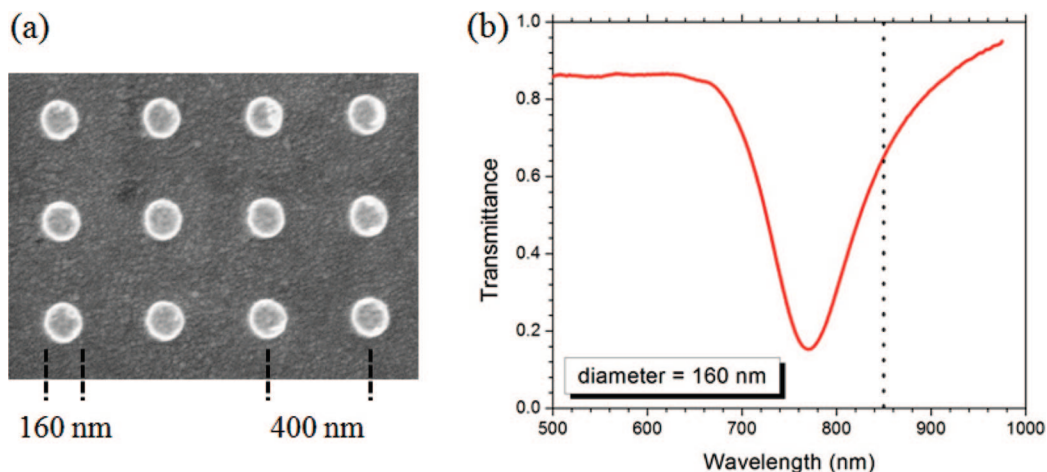


Figure 1. (a) SEM image of the Au nanoparticle array. Each nanoparticle is 160 nm in diameter and 40 nm in height, with lattice constant 400 nm. (b) Transmission spectrum of the array in air with the vertical line showing the sensor probe laser wavelength of 850 nm.

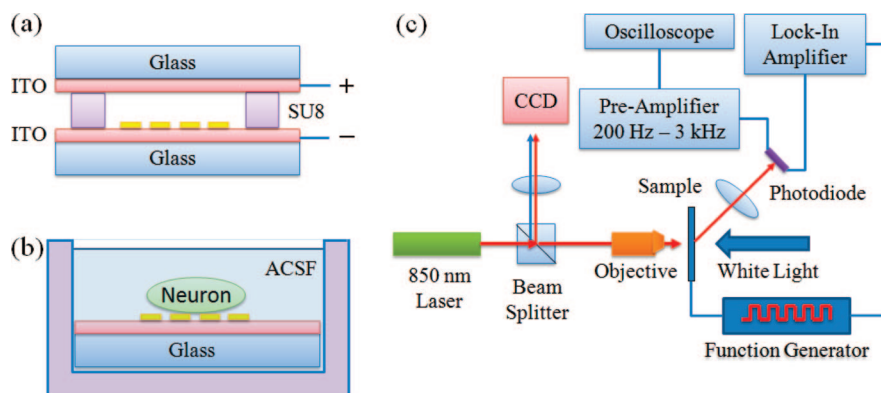


Figure 2. (a) Device structure for measuring the response of the “bare plasmonic” template to an external electrostatic field. The SU8 polymer spacer ring defines a circular microchamber filled with air. A modulating potential at 500 Hz was applied between the ITO plates. (b) The “plasmon/neuron” device where the perfusion chamber was filled with artificial cerebrospinal fluid (ACSF). (c) Schematic of overall optical experimental setup. White light was used to image the neural sample location onto a CCD camera for alignment. For bare plasmon samples, the scattering signal from the photodiode was fed into a lock-in amplifier. In the real-time neural measurements, the individual single cell switching was monitored by an oscilloscope after passing through a low-noise preamplifier set to pass 200 Hz to 3 kHz.

substrates using EBL patterning.³ These templates, composed of a high density of gold nanoparticles, were also used as substrates for the subsequent growth of neural cells to complete the neural sensor configuration. Here we focus on a specific plasmonic structure composed of a square array of pancake-shaped Au nanoparticles as shown in Figure 1a. Each nanoparticle is about 160 nm in diameter and 40 nm in height. The lattice constant of the array is 400 nm, with a total array area of $100 \times 100 \mu\text{m}$. A standard spectroscopic setup was first used to locate the LSP resonances, using incoherent white light at normal incidence. The transmission spectrum is displayed in Figure 1b (normalized with respect to the unpatterned areas of the substrate). The primary LSP resonance wavelength of the array is around 765 nm. The particular array used here is chosen such that the slope is large at the chosen probe laser wavelength of 850 nm, on the longer wavelength side of the transmission curve, which determines the sensitivity of the plasmonic array to a change in the metal dielectric constant, in the electric field sensor experiment. For the neuron-sensing experiment, the nano-

particle diameter was reduced to 140 nm so that the transmission spectrum in the biological solution (affected by the background dielectric constant change) was nearly identical to that in Figure 1b.

In order to quantify and model the LSP response of the planar arrays of Au nanoparticles in the presence of an applied electric/electrostatic field, we first constructed a device which housed the “bare plasmonic” template in the absence of any biological material. The device design and optical measurement setup are illustrated in Figure 2. The device (Figure 2a) consisted of two ITO-coated glass substrates separated by an insulating ring of SU8 polymer support layer (an epoxy based negative photoresist), which defined a $100 \mu\text{m}$ thick microchamber. The gold nanoparticle array was fabricated onto the bottom substrate. An electric potential difference at a modulation frequency of 500 Hz (similar to the typical neural cell dynamics) was applied between the two ITO substrates from a function generator. The output from an 850 nm diode laser was focused on the array at normal incidence, and the forward scattered light

was detected by a silicon photodiode at an angle of 50°. The photodiode output was fed into a lock-in amplifier.

The differential scattering signals ($\Delta S/S$) from the “bare plasmonic” template are plotted in Figure 3a for various applied voltages V_0 . The ac signal (ΔS) from the photodiode was measured with the lock-in amplifier, while the dc ($V_0 = 0$) signal ($S \sim 250$ mV) was monitored with an oscilloscope. The scattering signal is found to increase linearly with the applied voltage, at a rate of $\Delta S/SV_0 = 2.8 \times 10^{-6} \text{ V}^{-1}$. To describe the changes in the scattering signal in terms of variations in the applied voltage, we used the following model proposed by McIntyre¹⁵ and used by Lioubimov et al.¹⁴ in explaining the (propagating) SP resonance changes in a gold film under an oscillating electric potential.

Ignoring the capacitive effects, an applied potential V_0 across the ITO plates induces a surface charge density at the gold surface

$$\Delta\sigma = -\varepsilon_0 \frac{V_0}{d} \quad (1)$$

where ε_0 is the electric permittivity of vacuum and d is the distance between the plates (the plasmonic template is assumed to be at ground potential). Electrons are transferred from ITO to the gold nanoparticles, increasing the surface electron density. Assuming the change in the surface charge density is localized within the Thomas–Fermi screening length d_{TF} , the change in the electron number density N can be written as

$$\Delta N = -\frac{\Delta\sigma}{ed_{\text{TF}}} \quad (2)$$

where e is the elementary charge. The modulation of N results in a change in the gold plasma frequency $\omega_{\text{p}}^* = (e_2N/\varepsilon_0 m^*)^{1/2}$, where m^* is the effective electron mass. The change in ω_{p}^* is given by

$$\Delta\omega_{\text{p}}^* = \frac{\omega_{\text{p}}^*}{2N} \Delta N \quad (3)$$

For our purposes, the dielectric function of gold is well described by the Drude model

$$\varepsilon(\omega) = \varepsilon_\infty - \frac{\omega_{\text{p}}^{*2}}{\omega(\omega + i\gamma)} \quad (4)$$

where the static dielectric constant ε_∞ accounts for the background polarization due to the core electrons and γ is the characteristic collision frequency. The gold nanoparticles are approximated (in quasi-static approximation) as oblate spheroids with an aspect ratio of 0.25, whose polarizability is given by

$$\alpha = V \frac{\varepsilon(\omega) - \varepsilon_{\text{D}}}{L[\varepsilon(\omega) - \varepsilon_{\text{D}}] + \varepsilon_{\text{D}}} \quad (5)$$

where V is the volume of the particle, ε_{D} is the dielectric constant of the surrounding medium, and L is the geometrical factor in the polarization direction of the incident electromagnetic wave.¹⁶ For the resonance condition $\text{Re}[\varepsilon(\omega)] = \varepsilon_{\text{D}}(L - 1)/L$, the LSP resonance frequency can be found using eq 4

$$\omega_{\text{LSP}} = \sqrt{\frac{\omega_{\text{p}}^{*2}}{\varepsilon_\infty + \frac{1-L}{L}} - \gamma^2} \quad (6)$$

where we assume $\varepsilon_{\text{D}} \sim 1$. The change in the resonance frequency is

$$\Delta\omega_{\text{LSP}} = \frac{\omega_{\text{p}}^*}{\omega_{\text{LSP}} \left(\varepsilon_\infty + \frac{1-L}{L} \right)} \Delta\omega_{\text{p}}^* \quad (7)$$

Combining eqs 1–3 and 7, the shift in the resonance wavelength as a result of an applied voltage V_0 can be written as

$$\Delta\lambda_{\text{LSP}} = -\frac{\varepsilon_0 \omega_{\text{p}}^{*2} \lambda_{\text{LSP}}^3}{8\pi^2 c^2 N e d d_{\text{TF}} \left(\varepsilon_\infty + \frac{1-L}{L} \right)} V_0 \quad (8)$$

where λ_{LSP} is the LSP resonance wavelength and c is the speed of light in vacuum.

For the dielectric function of gold, we used the fitting parameters $\varepsilon_\infty = 9.07$, $\hbar\omega_{\text{p}}^* = 8.92$ eV, and $\hbar\gamma = 74$ meV (\hbar is Planck’s constant divided by 2π) of Vial et al.,¹⁷ found to work well around our LSP resonance wavelength of 765 nm. Substituting $\lambda_{\text{LSP}} = 765$ nm, $N = 5.9 \times 10^{22} \text{ cm}^{-3}$, $d = 100 \mu\text{m}$, $d_{\text{TF}} = 0.6 \text{ \AA}$,¹⁸ and $L = 0.15$ (corresponding to the aspect ratio of 0.25),¹⁹ one finds

$$\frac{\Delta\lambda_{\text{LSP}}}{V_0} = -1.25 \times 10^{-4} \text{ nm/V} \quad (9)$$

Since the LSP resonance shift is very small, the change in the shape of the transmission spectrum can be ignored and one can assume that the whole spectrum shifts rigidly by $\Delta\lambda = \Delta\lambda_{\text{LSP}}$. Approximating the scattered intensity by $S = 1 - T$, the differential scattering signal is given by

$$\frac{\Delta S/S}{V_0} = \frac{1}{1-T} \frac{\Delta T \Delta\lambda_{\text{LSP}}}{\Delta\lambda} \quad (10)$$

where $\Delta T/\Delta\lambda$ is the derivative of the transmission spectrum in Figure 1b. Equation 10 is plotted in Figure 3b as a function of wavelength. Although the model is intended to serve as an order-of-magnitude estimate (due to several approximations used), at the probing wavelength of 850 nm, the calculated value of $2 \times 10^{-6} \text{ V}^{-1}$ for $|\Delta S/SV_0|$ is comparable to that measured experimentally, $2.8 \times 10^{-6} \text{ V}^{-1}$ in Figure 3a.

In preparing the plasmonic nanoparticle templates for the neural cell experiment, they were first UV-sterilized for an hour and soaked in filtered poly-L-lysine (0.5 mg/mL in borate buffer solution) overnight. Tissue from the hippocampus of an E18 rat embryo was trypsinized at 37 °C for 15 min and subsequently dissociated by trituration in Hank’s balanced salt solution (HBSS) with 1% 4-(2-hydroxyethyl)-1-piperazineethanesulfonic acid (HEPES) and 1% penicillin–streptomycin. Digestion was terminated by changing the HBSS solution to Dulbecco’s modified eagle’s medium and fetal bovine serum (DMEM/FBS). Dissociated neurons were plated onto the plasmonic templates at an average density of ~ 5 cells/array. The templates were then placed inside an incubator with 5% CO_2 at 37 °C. After 3 h, the DMEM/FBS solution was changed to a serum-free medium contain-

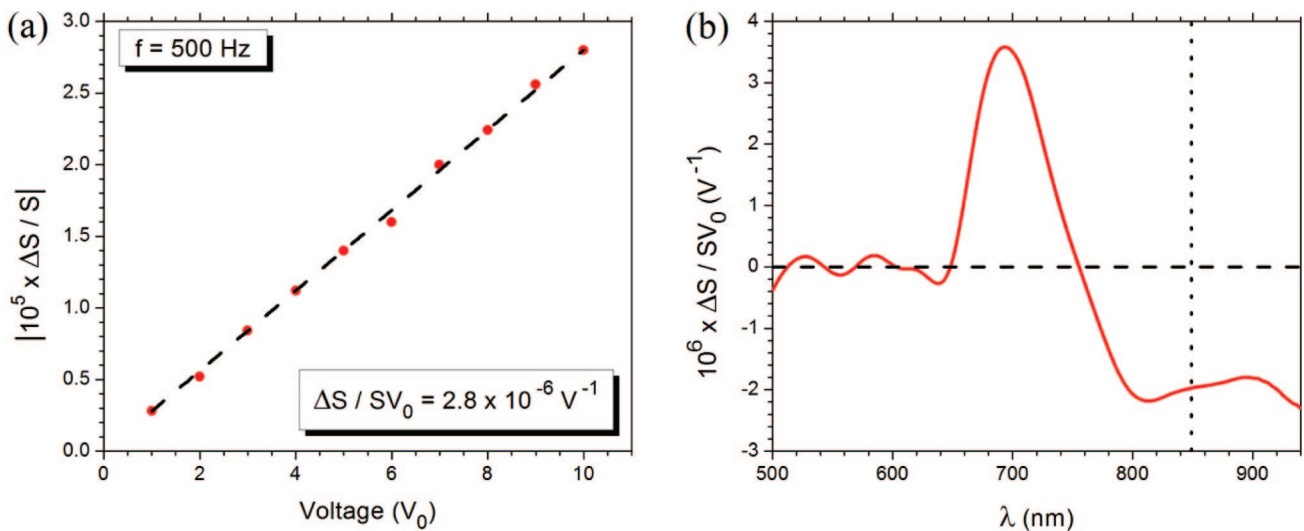


Figure 3. (a) Differential scattering signals from the “bare plasmonic” template. The modulation frequency is 500 Hz. The dashed line is a linear fit to the experimental data (circles) with slope = $|\Delta S|/SV_0 = 2.8 \times 10^{-6} \text{ V}^{-1}$. (b) Differential scattering signal per applied voltage for the same template, calculated using eq 10. $|\Delta S|/SV_0$ is around $2 \times 10^{-6} \text{ V}^{-1}$ at the probe laser wavelength of 850 nm.

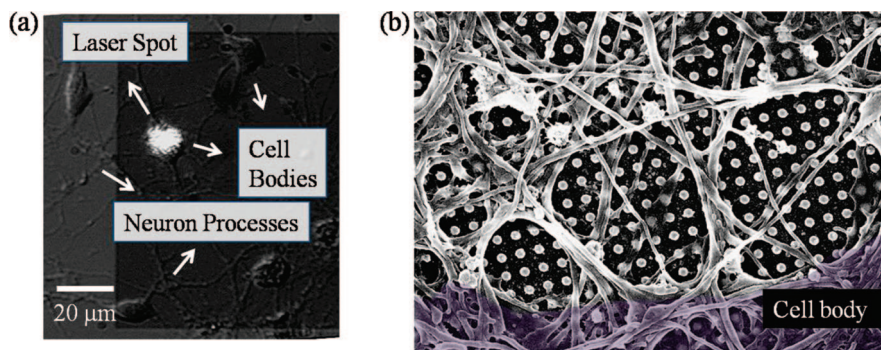


Figure 4. (a) Optical microscope image of the hippocampal neurons cultured on the plasmonic template at 16 DIV growth, showing neuron bodies (somas) and axons/dendrites (processes), as well as the size of the typical probe laser spot. (The Au-template region ($100 \times 100 \mu\text{m}$) produces a darker image). (b) SEM image of a hippocampal neuron cultured on the template at 14 DIV. The image shows part of the membrane at the edge of the cell body which is artificially colored and neural processes growing on top of the nanoparticle array. The lattice constant for the plasmonic probe array is 400 nm.

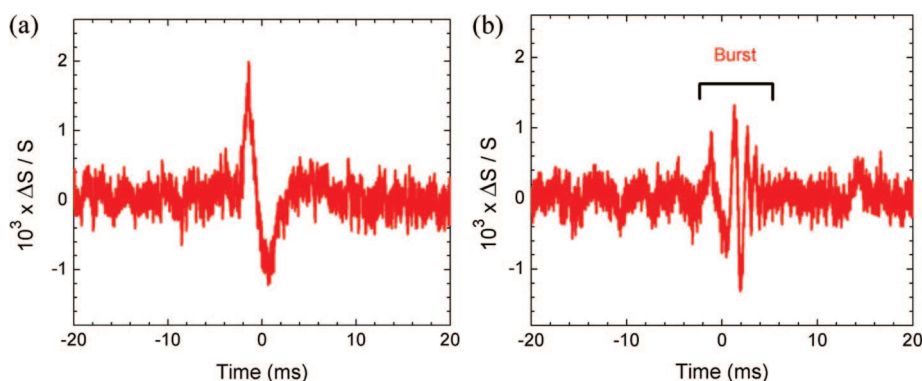


Figure 5. Differential scattering signals from the plasmon/neuron sample which shows (a) a single spike activity and (b) a burst of spikes. Each trace represents a single shot recording from a single neural cell.

ing Neurobasal media, 2% B27 serum-free supplement, 1% (penicillin–streptomycin), and 0.25% Glutamax, and fed twice a week for 2 weeks before the experiment. Figure 4a shows a microscope image of the dissociated hippocampal neurons cultured on a plasmonic template at 16 days in vitro (DIV). The smoothness of the cell bodies and the rich outgrowth of the neuronal “wiring” in the form of axons

and dendrites (known as “processes”) indicate the health of the neurons, which can be a challenge in preparing in vitro cultured specimen. There is no visual difference between the neurons resting atop the plasmonic template and those grown on the unpatterned area. An electron microscope (SEM) image of the sample is shown in Figure 4b, after dehydrating the cells.

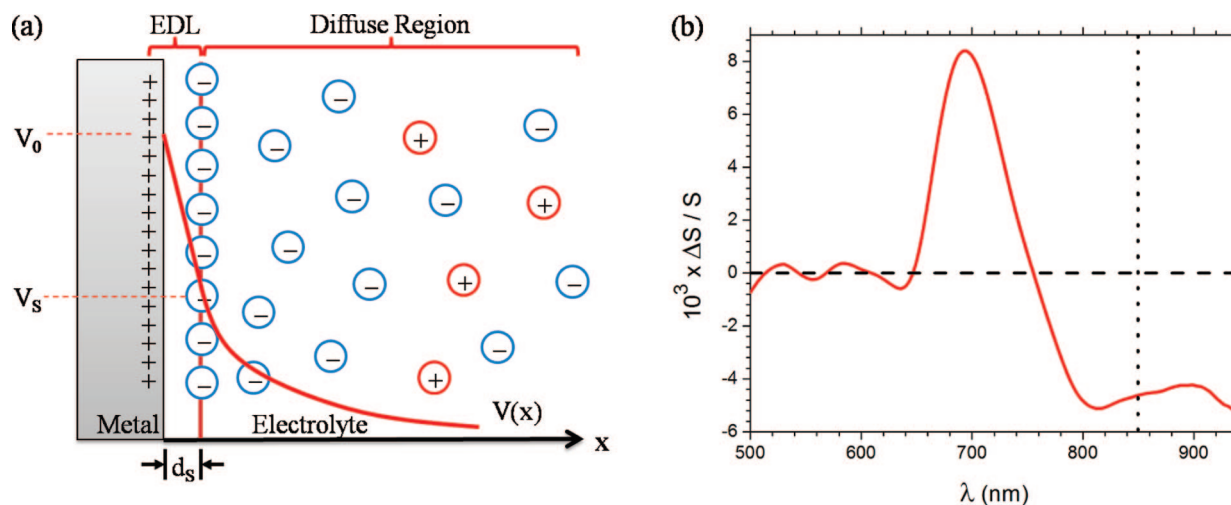


Figure 6. (a) Stern model for the Au–ACSF metal–electrolyte interface showing the EDL and diffuse regions. The gold electrode is at potential V_0 . The Stern layer potential is V_S . Thickness of the electrical double layer is d_s . (b) Differential scattering signal for the “plasmon/neuron” samples, calculated using eq 10. $\Delta\lambda_{LSP} = 0.293$ nm. T is taken from Figure 1b. $|\Delta S|/S$ is around 4.5×10^{-3} at the probing wavelength of 850 nm.

For the experiment, the plasmon/neuron sample was transferred from the incubator into a recording chamber (Figure 2b) filled with artificial cerebrospinal fluid (ACSF, 145 mM NaCl, 3 mM KCl, 3 mM CaCl₂, 1 mM MgCl₂, 10 mM glucose, and 10 mM HEPES). A 50 μ M portion of glutamate was injected into the ACSF to stimulate the neurons into spontaneous activity as approximately micro-second duration bursts of membrane potential “spikes” (action potentials).²⁰ A 40 \times water-immersion objective was used to focus the 850 nm laser light onto a given cell body, monitored by a CCD camera (Figure 2c). After passing through a low-noise preamplifier set to pass 200 Hz to 3 kHz, the forward scattering signal (ac) from the photodiode was monitored with an oscilloscope in real time (without averaging). A baseline monitoring of the neural cell activity showed that there were rarely any events in the scattered signal before the glutamate was injected. Spiking activity started to show up after the glutamate injection, and the oscilloscope was set to be triggered by any event which passed the threshold. A single spike and a burst of spikes from two different neurons (on different sites) are shown in Figure 5. The shape of the signals is typical of results that would be obtained in extracellular electrode recordings, in our experience. The signal amplitude varied slightly from neuron to neuron. We attribute it to the varying average distance between different neurons and the gold nanoparticle array, as well as the state of activity of the individual neuron. The spiking events started to die out about an hour after the glutamate injection, showing the degradation of the neural health.

To analyze the all-optical signals of Figure 5, we used the model described above with slight changes to account for the presence of the conducting ionic (electrolyte) solution. To describe the variation of the electric potential near the Au–ACSF (electrolyte) interface, we used the basic Stern model, illustrated schematically in Figure 6a. In this model, the ACSF solution near the gold surface is divided into two regions: the electrical double layer (EDL) and the diffuse

region. A molecular distance (~ 5 Å) away from the gold surface, a uniform layer of oppositely charged ions (the Stern layer) is formed. In the EDL region between the metal surface and the Stern layer, the potential change is linear. Beyond the Stern layer is the diffuse region that consists of a distribution of ions. The ion concentration decreases with increasing distance from the gold surface toward zero value. The potential at the Stern layer satisfies

$$V_S = V_0 - d_s \sqrt{\frac{8k_B T N_i}{\epsilon_S \epsilon_0}} \sinh \frac{zeV_S}{2k_B T} \quad (11)$$

where V_S is the Stern layer potential, V_0 is the surface potential, d_s is the EDL thickness, k_B is the Boltzmann constant, T is the absolute temperature, N_i is the known bulk concentration of ions, ϵ_S is the static dielectric constant of the ACSF solution, and z is the valence of the ions.¹⁴ Equation 11 can be solved graphically to find the electric field and the charge density at the gold surface.

The known experimental values for the extracellular action potential of a hippocampal neuron near the membrane range from 100 μ V up to a few millivolts, depending on both the physiological characteristics of the neuron (such as membrane resistance) and the distance of the probe from the membrane. We used an average extracellular potential of $V_0 = 500$ μ V in our calculations. For $d_s = 5$ Å,¹⁴ $k_B T = 26$ meV, $N_i = 145$ mM, $\epsilon_S = 80$, and $z = 1$, the Stern layer potential is found to be $V_S = 310$ μ V. The induced shift in the resonance wavelength is obtained from eq 8 making the substitutions

$$\frac{V_0}{d} \rightarrow \frac{\epsilon_S}{d_S} (V_0 - V_S), \quad \frac{1-L}{L} \rightarrow \frac{1-L}{L} \epsilon_D \quad (12)$$

where $\epsilon_D = 1.77$ is the dielectric constant of water and is found to be $\Delta\lambda_{LSP} = 0.293$ nm. Inserting this value into eq 10, the differential scattering signal is plotted in Figure 6b as a function of wavelength. At the probing wavelength of 850 nm, the calculated value of $\sim 4.5 \times 10^{-3}$ for $|\Delta S|/S$ is

comparable to those measured experimentally, $\sim 3 \times 10^{-3}$ in Figure 5.

We note that the amplitude of our measured and calculated scattering changes induced by neural cell spiking, on the order of 10^{-3} , is much larger compared to that acquired from the intrinsic (dielectric) birefringence change of the neuron on the order of 10^{-5} .^{12,21} The signals reported here are indeed comparable to those acquired by using voltage-sensitive fluorescent dyes (with similar millisecond time resolution), thus presenting a means of cellular recording of intrinsic neural material without additional chemical preparation or labeling.

In conclusion, we have shown how hippocampal neural spiking activity can be detected in real time by the LSP resonance shift in an embedded gold nanoparticle optical probe. Such a recording technique opens up the possibility of extending the use of metal nanoparticles for in vivo applications for all-optical recording. Our technique has the scalability in detecting multiple neuron activities in neural microcircuits according to the geometry of the plasmon probe array. In planning for in vivo experiments, one important consideration is the delivery of the plasmonic nanoparticles to deeper brain tissue. Colloidal nanoparticles might play a useful role here. It has been demonstrated that chemically functionalized nanoparticles (such as neuropeptide-attached nanoparticles coated with polysorbate 80) can be delivered to the neural tissue through the blood–brain barrier via receptor-mediated endocytosis.²² Nanoparticle arrays can also be fabricated onto the facet of an optical fiber by focused ion beam,²³ which could then be implanted into the brain. Moreover, while traditional two-photon microscopy can be used to image subcellular features such as a single dendritic spine using Calcium dyes, it is nonetheless limited by optical diffraction.²⁴ A nanoparticle-based plasmonic sensor can provide an opportunity for optically probing local neural activity on submicron scale where local membrane ion channels operate.

Acknowledgment. Research was supported by Grants from the National Science Foundation (0725740) and Department of Energy (ER 46387).

References

- (1) Hiroharu, T.; Hitoshi, K.; Hideki, T. M.; Kenjiro, M. *Appl. Phys. Lett.* **2002**, *80*, 1826–1828.
- (2) Lamprecht, B.; Krenn, J. R.; Leitner, A.; Aussenegg, F. R. *Phys. Rev. Lett.* **1999**, *83*, 4421.
- (3) Atay, T.; Song, J. H.; Nurmikko, A. V. *Nano Lett.* **2004**, *4*, 1627–1631.
- (4) Williams, J. C.; Rennaker, R. L.; Kipke, D. R. *Brain Res. Protoc.* **1999**, *4*, 303–313.
- (5) Buzsaki, G. *Nat. Neurosci.* **2004**, *7*, 446–451.
- (6) Nordhausen, C. T.; Maynard, E. M.; Normann, R. A. *Brain Res.* **1996**, *726*, 129–140.
- (7) Chang, J. C.; Brewer, G. J.; Wheeler, B. C. *Biomed. Microdevices* **2000**, *2*, 245–253.
- (8) Bullen, A.; Saggau, P. *Biophys. J.* **1999**, *76*, 2272–2287.
- (9) Svoboda, K.; Denk, W.; Kleinfeld, D.; Tank, D. W. *Nature* **1997**, *385*, 161–165.
- (10) Venkataramani, S.; Davitt, K. M.; Zhang, J.; Xu, H.; Song, Y.-K.; Connors, B. W.; Nurmikko, A. V. *IEEE J. Sel. Top. Quantum Electron.* **2005**, *11*, 785–790.
- (11) Cao, Y. C.; Jin, R.; Mirkin, C. A. *Science* **2002**, *297*, 1536–1540.
- (12) Kim, A. S.; Byun, M. K.; Lee, J.; Kim, H. J.; Kim, Albert, D.-G.; Baac, H.; Shuler, M. L.; Kim, J. S. *Opt. Lett.* **2008**, *33*, 914–916.
- (13) Song, Y.-K.; Stein, J.; Patterson, W. R.; Bull, C. W.; Davitt, K. M.; Serruya, M. D.; Zhang, J.; Nurmikko, A. V.; Donoghue, J. P. *J. Neural Eng.* **2007**, *4*, 213–218.
- (14) Lioubimov, V.; Kolomenskii, A.; Mershin, A.; Nanopoulos, D. V.; Schuessler, H. A. *Appl. Opt.* **2004**, *43*, 3426–3432.
- (15) McIntyre, J. D. E. *Surf. Sci.* **1973**, *37*, 658–682.
- (16) Gans, R. *Ann. Phys. (Leipzig)* **1912**, *37*, 881–900.
- (17) Vial, A.; Grimault, A.-S.; Macias, D.; Barchiesi, D.; de la Chapelle, M. L. *Phys. Rev. B: Condens. Matter Mater. Phys.* **2005**, *71*, 085416–085417.
- (18) Ekanayake, S. R.; Ford, M.; Cortie, M. *Mater. Forum* **2004**, *27*, 15–20.
- (19) Hulst, H. *Light Scattering by Small Particles*; Dover Publications: New York, 1981.
- (20) Venkataramani, S.; Davitt, K. M.; Xu, H.; Zhang, J.; Song, Y.-K.; Connors, B. W.; Nurmikko, A. V. *J. Neurosci. Methods* **2007**, *160*, 5–9.
- (21) Stepnoski, R. A.; LaPorta, A.; Raccuia-Behling, F.; Blonder, G. E.; Slusher, R. E.; Kleinfeld, D. *Proc. Natl. Acad. Sci.* **1991**, *88*, 9382–9386.
- (22) Silva, G. A. *Surg. Neurol.* **2007**, *67*, 113–116.
- (23) Smythe, E. J.; Cubukcu, E.; Capasso, F. *Opt. Express* **2007**, *15*, 7439–7447.
- (24) Nimchinsky, E. A.; Yasuda, R.; Oertner, T. G.; Svoboda, K. *J. Neurosci.* **2004**, *24*, 2054–2064.

NL801891Q